**Article:**

Liang, R, Schruff, T, Jia, X et al. (2 more authors) (2015) Validation of a stochastic digital packing algorithm for porosity prediction in fluvial gravel deposits. Sedimentary Geology, 329. 18 - 27. ISSN 0037-0738

https://doi.org/10.1016/j.sedgeo.2015.09.002

# Validation of a stochastic digital packing algorithm for porosity prediction in fluvial gravel deposits

Rui Liang [a,*], Tobias Schruff [a], Xiaodong Jia [b], Holger Schüttrumpf [a], Roy M. Frings [a]

[a] Institute of Hydraulic Engineering and Water Resources Management, RWTH Aachen University, Aachen D 52056, Germany
[b] Institute of Particle Science and Engineering, School of Process, Environmental and Materials Engineering, University of Leeds, Leeds LS2 9JT, UK
[*] Corresponding author. Tel.: +49 (0)241 80 25757; Fax: +49 (0)241 80 25750. E-Mail address: rui@iww.rwth-aachen.de (R. Liang).

**Abstract**

Porosity as one of the key properties of sediment mixtures is poorly understood. Most of the existing porosity predictors based upon grain size characteristics have been unable to produce satisfying results for fluvial sediment porosity, due to the lack of consideration of other porosity-controlling factors like grain shape and depositional condition. Considering this, a stochastic digital packing algorithm was applied in this work, which provides an innovative way to pack particles of arbitrary shapes and sizes based on digitization of both particles and packing space. The purpose was to test the applicability of this packing algorithm in predicting fluvial sediment porosity by comparing its predictions with outcomes obtained from laboratory measurements. Laboratory samples examined were two natural fluvial sediments from the Rhine River and Kall River (Germany), and commercial glass beads (spheres). All samples were artificially combined into seven grain size distributions: four unimodal distributions and three bimodal distributions. Our study demonstrates that apart from grain size, grain shape also has a clear impact on porosity. The stochastic digital packing algorithm successfully reproduced the measured variations in porosity for the three different particle sources. However, the packing algorithm systematically overpredicted the porosity measured in random dense packing conditions, mainly because the random motion of particles during settling introduced unwanted kinematic sorting and shape effects. The results suggest that the packing algorithm produces loose packing structures, and is useful for trend analysis of packing porosity.

**Keywords:** Porosity; Sediment; Grain shape; Random packing; Rivers

## 1. Introduction

Porosity prediction of sedimentary deposits is of interest in a fluvial environment. Previous studies have shown that porosity, as a key structural property, plays an important role in the morphological, ecological and geological characteristics of fluvial systems. Morphologically, porosity governs the initiation of sediment motion and bank collapse (e.g., Wilcock, 1998; Vollmer and Kleinhans, 2007). Ecologically, porosity determines the interstitial space of the hyporheic zone for aquatic habitats (e.g., Boulton et al., 1998). Geologically, porosity dominates the exploitable reserve of oil, gas, and groundwater stored in the voids of fluvial deposits (e.g., Athy, 1930). To date, existing porosity predictors can generally be classified into two types: (1) empirical predictors; and (2) theoretical predictors. Most efforts to predict porosity have been empirically driven, to a large extent based upon median grain size $D_{50}$ (e.g., Carling and Reader, 1982; Wu and Wang, 2006), sorting coefficient σ (e.g., Wooster et al., 2008), or a combination of different grain size characteristics (e.g., Frings et al., 2011; Desmond and Weeks, 2014). Theoretical predictors such as geometrical models (e.g., Ouchiyama and Tanaka, 1984; Suzuki and Oshima, 1985) or analytical models (e.g., Yu and Standish, 1991; Koltermann and Gorelick, 1995; Esselburn et al., 2011) relate porosity to the full grain size distribution of perfect spheres. The performance of these predictors has been investigated by comparing porosity values measured in situ with those computed by the predictors (e.g., Frings et al., 2008, 2011). Unfortunately, these predictors produced unsatisfying results in predicting fluvial sediment porosity (Frings et al., 2011), probably because such predictors mainly focused on grain size characteristics, ignoring other porosity-controlling factors such as depositional environment and grain shape.

Effects of grain shape on porosity have received less attention, due to the complexity of arbitrary shapes of natural particles. Over the past decade, the application of computer simulations for the study of granular particle packings has become more popular, supported by developments in the computer hardware industry. However, most of the computer simulations have been limited to simple analytical geometries such as cylinders (Zhang et al., 2006), disks (Desmond and Weeks, 2009), ellipsoids (Donev et al., 2007; Zhou et al., 2011) and spherocylinders (Abreu et al., 2003; Williams and Philipse, 2003; Zhao et al., 2012). The major reason is the practical difficulty of representing and handling irregular shapes using vector-based approaches. Traditional ways to construct an irregular particle require the user to place spherical elements within a meshed polyhedral body (e.g., Wang et al., 2007; Matsushima et al., 2009; Ferellec and McDowell, 2010; Fukuoka et al., 2013), which consumes high computational costs with large numbers of components (spheres) involved (Hubbard, 1996; Song et al., 2006). Although techniques using 3D polyhedral (Latham et al., 2001) or continuous superquadric functions (Williams and Pentland, 1992; Lu et al., 2012) provide a straightforward way to generate irregular particle shapes, complex contact-detection algorithms are needed, leading to deterioration in simulation speed as particle complexity increases (Johnson et al., 2004).

In order to overcome these difficulties, a stochastic digital packing algorithm was developed (Jia and Williams, 2001). The packing algorithm is distinguished from the traditional vector-based packing models by digitization of both particles and packing space, allowing for a much easier and computationally efficient way to pack particles of irregular shapes with no more than an ordinary PC. These advantages make it attractive to create packings of complex fluvial deposits, and to study the grain shape effects on porosity. Applications of this stochastic digital packing algorithm have proven to provide relatively accurate porosity predictions for both fine powders (Jia et al., 2007) and large spheres (Caulkin et al., 2006, 2007) in the fields of material science and engineering chemistry. Nevertheless, the packing algorithm has not yet been used for generating packings of fluvial deposits. Therefore, the primary purpose of this work was to test the applicability of the stochastic digital packing algorithm in predicting fluvial sediment porosities. In this study, we focused on fluvial gravel mixtures and did so by comparing the predicted porosities with those obtained from laboratory measurements.

## 2. Materials and methods

### 2.1. Particle acquisition and analysis

The particles employed for this study came from three different sources: (1) fluvial gravels from the Rhine River (Germany), (2) fluvial gravels from the Kall River (Germany), and (3) commercial glass beads. The Rhine sediments were collected from the channel bed between the barrage of

Iffezheim and the German-Dutch border between July 2008 and April 2011. Quartz is the dominant lithology. The Kall sediments were collected from the channel bed near the river mouth in June 2014. Slate is the dominant lithology.

After acquisition, the fluvial sediments were carefully cleaned by flushing with fresh water, dried in an oven at 105 °C for 48 h and sieved into seven size fractions: 2.8-4 mm, 4-5.6 mm, 5.6-8 mm, 8-11.2 mm, 11.2-16 mm, 16-22.4 mm, 22.4-31.5 mm. Subsequently, these fractions were combined into seven grain size distributions: four unimodal ones with logarithmic standard deviations ($\sigma_\varphi$) of 0.00, 0.32, 0.49 and 0.71, and three bimodal ones, with the finer mode, making up either k=30, k=50 or k=70 percent of the distribution (Fig. 1). The glass beads with seven size fractions of 3, 4, 6, 8, 11, 16 and 22 mm were also combined into the same distributions as above.

For the fluvial sediments, nine representative particles were chosen based on visual judgments from each of the seven sieve fractions, and digitized (Fig. 2) using a nonmedical X-ray computed tomography (CT) scanner. Shape analysis was done according to the classic Zingg diagram (Zingg, 1935), which categorizes particle shape into sphere, disc, blade and rod categories on the basis of the elongation ratio (b/a) and flatness ratio (c/b), where a, b and c are the long, intermediate and short orthogonal axes respectively of the smallest volume imaginary box that can contain the particle (Blott and Pye, 2008). It can be seen in Figure 3 that most of the Rhine sediments locate within the sphere area while the Kall sediments are dominated by disks and blades. According to Krumbein's (1941) equation

(1), the intercept sphericity ($\psi$) for each selected particle was calculated, with an average intercept sphericity of 0.74 gained for the Rhine sediments and 0.55 for the Kall sediments.

$$\psi = \sqrt[3]{\frac{b*c}{a^2}} \qquad (1)$$

2.2. Laboratory porosity measurements

The water displacement method (Bear, 1972) was used for porosity measurements. The experimental procedure was as follows: firstly, a plastic cylinder with an inner diameter of 104 mm was partially filled with a known volume of water $V_w$ larger than the expected pore volume of the particles to be added. Then, particles of 3 kg mass were added into the cylinder in small well-mixed portions, together with gently tapping the side of the cylinder in order to dislodge trapped air bubbles and obtain a stable, dense packing. The final water level was visually read to obtain the whole accumulated volume $V_a$ ($V_a$ = $V_w$ + $V_s$, where $V_s$ is the volume of the solid fraction). The jagged surface of the particle packing caused by the wide range of sizes and shapes was then smoothed by hand and the total volume of the particle packing $V_t$ (including pores) was obtained through reading the height of the particle packing. Eventually, the porosity was computed as $n = V_p/V_t$, where $V_p$ ($= V_t - (V_a - V_w)$) is the pore volume of the particle packing.

In total, 42 laboratory porosity experiments were performed as a basis for the validation of the stochastic digital packing algorithm: 14 experiments with the sub-spherical Rhine sediments (7 distributions, each two times), 14 experiments with low-sphericity Kall sediments (again 7×2) and 14 experiments with the spherical glass beads (again 7×2).

## 2.3. Porosity simulation

The stochastic digital packing algorithm of Jia and Williams (2001) is designed to pack particles of arbitrary sizes and shapes in a confined space of arbitrary geometry. In this packing algorithm, every element is digitized: each particle as a coherent collection of voxels, the packing space (in a container) as a lattice grid, and the movements take place in units of grid cells. During the simulation, the movements of particles, both translational and rotational, are random. In 3D, there are 26 possible translational directions: 6 orthogonal and 20 diagonal. The diagonal moves are treated as a combination of two orthogonal moves. To ensure particles settle while still make use of every available space, a rebounding probability is used. An upward movement (which may be an orthogonal move or part of a diagonal move) is only realized with this probability. After translation, a trial rotation follows, and it is accepted if the rotation does not result in overlaps. Compared with vector-based approaches and for complex shapes, this digital approach is advantageous in several respects. First, there is no conversion or parameterization required, since objects digitized by modern imaging devices, such as X-ray tomography (e.g., Richard et al., 2003) or nuclear magnetic resonance imaging (e.g., Kleinhans et al., 2008), are already in the digital volumetric format required by the packing algorithm. Secondly, collision and overlap detection (normally the most computationally expensive part of packing simulations) is much easier to implement as computer code, and usually faster to execute for complex shapes. Thirdly, the number of voxels used to represent objects, and hence to a large extent the simulation runtime, does not necessarily increase with shape complexity. The reverse is also true: it does not necessarily reduce with shape simplification either. Further details on the stochastic digital packing algorithm can be found elsewhere (Jia and Williams, 2001; Caulkin et al., 2006, 2007).

In order to produce porosity results comparable to those aforementioned measurements, simulation conditions need to be set up to resemble the laboratory experiments, with respect to the packing space, the particle mixtures and the packing process. The digital objects (i.e., packing space and particles) were prepared with DigiUtility, which is a bundled tool for viewing, manipulating and preparing digital files for this packing algorithm. In DigiUtility, a cylinder (packing space) with solid boundary was built with the size of 104 mm in diameter, and 300 mm in height, which is slightly higher than the largest real packing heights (about 250 mm) to ensure all the particles would drop into it. The particle mixtures (i.e., number of particles in each of the fractions) employed in these simulations were derived on a weight-to-weight basis. For glass beads, the numbers of particles in each fraction were determined as the ratio of the real mass of each fraction to the single particle mass (density of 2500 kg/m$^3$ used for glass beads). The regular spherical shapes with different sizes were directly created in digital formats using DigiUtility. In the case of the fluvial sediments, we used nine digitized typical particles to represent each fraction and repeated them as many times as needed to make up the feedstock according to the required grain size distributions. The density of fluvial gravels was set to 2650 kg/m$^3$. Resolution of 0.5 mm/voxel for the digital objects was assigned as it offers relatively precise representation of the real particles in both dimension and shape, and also limits the computational cost to a feasible amount.

Having the digital objects created, a range of options and parameters was set to mimic the packing process. The source was set to “rain-dropping” mode to let the particles randomly drop from a circular area above the cylinder. In addition to the translational movements, particles were also allowed to rotate randomly during the simulation. Optimized values of the parameters (rebounding probability, addition rate and number of time steps) that control the generated packing structures were chosen such as to create the densest possible packings. By doing so, simulation conditions (Table 1) matched the experimental setups as close as possible. Finally, the porosity of the digital packings was determined as the ratio of the number of empty voxels to the total number of voxels within the corresponding packing space. Porosity was calculated for the lower 90% of the mixture to exclude effects of surface irregularities. Each simulation was also done twice and 42 simulations were achieved in total.

## 3. Results

### 3.1. Measured porosity

The porosity measured in the laboratory experiments is shown in Figure 4. For the unimodal particle mixtures, porosity decreases with increasing logarithmic standard deviations, while the bimodal particle mixtures generally have lower porosity than the unimodal mixtures. This variation in porosity reflects the mixing effect between small and large particles.

Porosity comparisons between the three different particle sources show the low-spherical Kall sediments and the spherical glass beads produced higher porosity than the sub-spherical Rhine sediments, which confirms that there is a decrease and then increase in porosity as particle shape varies from spherical to platy (Tickell and Hiatt, 1938; Zou and Yu, 1996). On the other hand, in the case of the bimodal particle mixtures, different tendencies toward the porosity are appreciable (Fig. 4B), suggesting grain shape exerts a quite complicated influence on porosity, not merely in variation of amount but in variation of trend.

It should be noted that the dense sediment deposits packed by hand in the laboratory experiments are not fully representative of natural situations where grain arrangement is determined by depositional conditions, such as flow impact (with near-bed turbulence playing an important role) and burial depth (compaction mechanism). This topic is beyond the current effort. Nonetheless, based on the comparisons between field measurements of porosity in the River Rhine (28 measurements on the channel bed and 18 measurements on the river banks, focusing on subsurface sediments) and measurements in the laboratory (Frings et al., 2011), it was found that in most cases (59%), the difference between is less than 0.03 (Fig. 5), with an average porosity of 0.24 obtained ex situ and 0.22 in situ.

## 3.2. Algorithm behavior

The behavior of the stochastic digital packing algorithm is presented in Figure 6. In order to validate the packing algorithm, comparisons were made between the measured and simulated porosity outcomes. Figure 7 clearly shows that the packing algorithm successfully captures the measured variation in porosity due to grain size distributions for each particle source. While the packing algorithm also seems to be able to mimic the measured variation due to grain shape for a given grain size distribution, providing that the glass beads (spheres) are not taken into account (Fig. 8).

However, nearly all simulated porosities were systematically overestimated compared to the experimental measurements. To easily recognize these discrepancies, relative errors between the measured and simulated porosities were calculated (Table 2). The average relative error is 29.4% for the Rhine sediments, 21.7% for the Kall sediments and 6.6% for the glass beads, indicating that the packing algorithm predicted relatively higher porosities when it comes to fluvial sediments with irregular shapes. Figure 9 shows the comparison between these discrepancies over the seven grain size distributions. For the unimodal particle mixtures, the discrepancies are growing as logarithmic standard deviation increases (Fig. 9A). For the bimodal particle mixtures, with the finer mode increasing from 30% to 70%, the discrepancies for fluvial sediments decrease while the discrepancies for glass beads increase (Fig. 9B).

## 4. Discussion

The purpose of determining the porosities of the samples was twofold: first, to point out that apart from grain size, grain shape also has a clear impact on porosity (shown in section 3.1), and second, to serve as a basis of comparison for the porosities predicted from the stochastic digital packing algorithm. It is shown in section 3.2 that although the packing algorithm is able to follow the experimental trend, systematic overestimation of the porosity is noticeable, especially for the fluvial sediments. The remarkable discrepancies between can be caused by (1) measurement inaccuracies, and/or (2) simulation inaccuracies.

### 4.1. Measurement inaccuracies

For the laboratory measurements, the reading errors related to the water levels and packing heights dominate the accuracy of outputs. The water levels were visually read to obtain the whole accumulated volumes $V_a$ with a deviation of about 1 mm, and readings of the packing heights for gaining the total volume of particle packing $V_t$ (including pores) were achieved with an accuracy of ~3 mm. These inevitable reading errors can lead to the absolute error of the porosity to be ~0.01 for the measurements. However, measured inaccuracies are small compared to the apparent differences between the measured and simulated porosities, particularly for fluvial sediments.

### 4.2. Simulation inaccuracies

#### 4.2.1. Digitization inaccuracy

As can be seen in Figure 10, the arrangements of particles leave unexpected pore spaces. One reason for this may be the digitization errors of digital objects represented at a resolution of 0.5 mm/voxel. The effect can be supported by the fact that the porosity of 0.355 simulated for glass beads is less than the limit of 0.36 in a random dense packing of spheres (Scott, 1960; Allen, 1985; Yu and Standish, 1991; Weltje and Alberts, 2011). This is probably because the spherical shape of glass beads is not perfectly described at such a resolution (0.9% digitization error), causing a reduction of porosity. Korte and Brouwers (2013) also observed the same effects in the simulation of packing 3D digitalized spheres under different resolutions. For this reason, a test for the ID 5 case (Table 2) was carried out with a higher resolution of 0.25 mm/voxel to decrease the digitized errors, especially for smaller particles. This gave a slightly lower porosity of 0.37 instead of 0.38 at 0.5 mm/voxel resolution, indicating that effects of digitization errors are not too significant when compared to the discrepancies between measured and simulated porosities.

Another error arises from the strict non-overlap requirement in the algorithm. Imagine two large objects side by side. If for any reason, there is a voxel protruded from either of the objects, this single voxel can stop the two objects from coming closer, thus leaving a large gap. In reality or in DigiDEM simulations, where forces instead of probabilities are used to determine in which direction and by how much each object moves in the next time step, this would not have happened.

4.2.2. Process control parameters

Another cause of simulation inaccuracy is the settings of process control parameters that affect the simulated packing structures, which are rebounding probability, addition rate and number of time steps. We did a sensitivity analysis to define the effects of these parameters on porosity. This was done by running a number of simulations in which one of the parameters was varied while keeping the others constant. To perform these simulations, 750 spherical particles (6.4 mm in diameter) and a cylinder (64mm in both diameter and height) were used. Resolution was set to 0.4 mm/voxel, giving a slight difference (<1% digitization error) between the digital volumes and real volumes.

Rebounding probability, designed to allow particles to move upwards, provides a non-physical way to generate vertical vibrations. The original intention of having a rebounding probability is to make it possible for particles to escape from their cramped places and continue to explore more suitable space to fit in, thereby simulating sediment compaction. The rebounding probability can be set between 0 and 1. A value of 0 means no rebounding and hence no vertical vibration applied. A value of 1 means particles having the same probability to move up or down, and hence kept suspended. To investigate its effects on porosity, seven rebounding probabilities varying from 0.1 to 0.7 were tested, while the addition rate and number of time steps remained the same (Table 3). The sensitivity analysis shows that bulk porosities vary parabolically as a function of the rebounding probability (Fig. 11A). The lowest porosity values appear at rebounding probabilities of 0.3-0.5, while lower and higher rebounding probabilities give higher porosities.

Addition rate controls the speed of introduction of particles into the packing space. Simulations with seven fixed addition rates were performed with the same sets of rebounding probability, and number of time steps (Table 4). Slower addition rates tend to generate denser packing structures, with bulk porosities decreasing from 0.46 to 0.42 (Fig. 11B). This effect is because with slower addition rates, particles have more time to find a better fitting position before being locked-in by new additions, resulting in denser packing structures.

In the packing algorithm, three types of time steps are defined: normal time steps, extra time steps and wind up time steps. Normal time steps are those during which particles drop into the packing space. They are closely related to the addition rate. For example, if the addition rate is chosen such that one particle drops down every 10 time steps, 1000 normal time steps are needed to introduce 100 particles into the packing space. In the case that a previously introduced particle still remains on top of the container, the next particle might be prevented from being introduced. In this instance, the next particle has to "wait" and extra time steps are needed to finish the packing. Wind up time steps are time steps at the end of a simulation during which no more particles are added and the rebounding probability is set to zero. These time steps enable the whole packing structure to consolidate. During the sensitivity analysis, only the effect of wind up time steps on porosity was assessed, since the effect of normal and extra time steps is directly related to the addition rate. The number of wind up time steps was varied between 0 and 32000 (Table 5), and shows no systematic effect on porosity (Fig. 11C).

The sensitivity analysis confirms that the settings we chose for the validation of the stochastic digital packing algorithm (Table 1) result in the densest possible packings. This shows that the overestimation of porosity by this packing algorithm cannot be solved by choosing different settings for the simulations.

4.2.3. Random walk-based algorithm

The reasons why the simulations failed to yield random dense packing structures can be explored in the random walk-based packing algorithm, by which the translational and rotational movements of particles during the simulation are completely random. Looking at the cross sections of the digital packings (Fig. 10) closely, the mixing of the particles is not uniform as smaller particles are more likely to concentrate at the bottom layer, particularly for the bimodal distributions with percentage of small particles increasing from 30% up to 70%. The phenomenon can be interpreted by kinematic sorting (i.e., segregation) effects. This is because particles kept moving randomly throughout the simulation, thus giving more chances for smaller particles to move through the pore spaces between larger particles and reach the bottom layer. Observations from Figure 10 also suggest that shape effects strongly affect the simulated packing structures of fluvial sediments compared to the packings of glass beads. Because of random rotational motions during the simulation, the arrangements of particles with irregular shapes lead to create larger voids, especially between larger particles. For the simulations of glass beads, shape effects are inconsequential because the rotation of a sphere has no impact on particle packing. Therefore, kinematic sorting can fully explain the growing discrepancy trend for glass beads over the seven grain size distributions, while shape effects are the dominant reason that causes the porosity to be significantly overestimated for fluvial sediments (Fig. 9).

## 5. Conclusions

The applicability of a stochastic digital packing algorithm in predicting porosity of fluvial gravel deposits was validated. The conclusions are summarized as follows: (1) Apart from grain size, grain shape has a clear impact on porosity. (2) The packing algorithm provides an innovative way to simulate fluvial sediment mixtures with arbitrary shapes. (3) The packing algorithm correctly reflects the mixing effect on porosity for unimodal particle mixtures and also reproduces the differences in porosity for bimodal particle mixtures. However, in all cases, the packing algorithm systematically overestimates porosity mainly due to the unwanted kinematic sorting effects as well as shape effects introduced by the random motion of particles. (4) The packing algorithm is useful for trend analysis of packing porosity; but for a quantitative match a more rigorous model such as Discrete Element Method (DEM) where particle motion is physics-based may be needed.

## Acknowledgments

We thank Alejandro Calatayud, Isabelle Schmidt and Ferdinand Habbel for the pleasant cooperation during the laboratory experiments, and also Thomas Fischer and Rodrigo Guadarrama-Lara for the assistance to the digitization of Rhine and Kall sediments.

## References


Abreu, C.R.A., Tavares, F.W., Castier, M., 2003. Influence of particle shape on the packing and on the segregation of spherocylinders via Monte Carlo simulations. Powder Technology 134, 167-180.

Allen, J.R.L., 1985. Principles of Physical Sedimentology. Allen and Unwin, London.

Athy, L.F., 1930. Density, porosity, and compaction of sedimentary rocks. AAPG Bulletin 14, 1-24.

Bear, J., 1972. Dynamics of Fluids in Porous Media. Dover Publications, New York.

Blott, S.J., Pye, K., 2008. Particle Shape: a review and new methods of characterization and classification. Sedimentology 55, 31-63.

Boulton, A.J., Findlay, S., Marmonier, P., Stanley, E.H., Valett, H.M., 1998. The functional significance of the hyporheic zone in streams and rivers. Annual Review of Ecology, Evolution, and Systematics 29, 59-81.

Carling, P.A., Reader, N.A., 1982. Structure, composition and bulk properties of upland stream gravels. Earth Surface Processes and Landforms 7, 349-365.

Caulkin, R., Fairweather, M., Jia, X., Gopinathan, N., Williams, R.A., 2006. An investigation of packed columns using a digital packing algorithm. Computers and Chemical Engineering 30, 1178-1188.

Caulkin, R., Ahmad, A., Fairweather, M., Jia, X., Williams, R.A., 2007. An investigation of sphere packed shell-side columns using a digital packing algorithm. Computers and Chemical Engineering 31, 1715-1724.

Desmond, K.W., Weeks, E.R., 2009. Random close packing of disks andspheres in confined geometries. Physical Review E 80, 051305, doi: 10.1103/PhysRevE.80.051305.

Desmond, K.W., Weeks, E.R., 2014. Influence of particle size distribution on random close packing of spheres. Physical Review E 90, 022204, doi: 10.1103/PhysRevE.90.022204.

Donev, A., Connelly, R., Stillinger, F.H., Torquato, S., 2007. Underconstrained jammed packings of nonspherical hard particles: Ellipses and ellipsoids. Physical Review E 75, 051304, doi: 10.1103/PhysRevE.75.051304.

Esselburn, J.D., Robert, W.R.J., Dominic, D.F., 2011. Porosity and permeability in ternary sediment mixtures. Ground Water 49, 393-402.

Ferellec, J., McDowell, G., 2010. Modeling realistic shape and particle inertia in DEM. Géotechnique 60, 227-232.

Frings, R.M., Kleinhans, M.G., Vollmer, S., 2008. Discriminating between pore-filling load and bed-structure load: a new porosity-based method, exemplified for the river Rhine. Sedimentology 55, 1571-1593.

Frings, R.M., Schüttrumpf, H., Vollmer, S., 2011. Verification of porosity predictors for fluvial sand-gravel deposits. Water Resources Research 47, W07525, doi: 10.1029/2010WR009690.

Fukuoka, S., Nakagawa, H., Sumi, T., Zhang, H., 2013. Advances in River Sediment Research, Taylor and Francis Group, London, pp. 323-332.

Hubbard, P.M., 1996. Approximating polyhedra with spheres for time-critical collision detection. ACM Transactions on Graphics 15, 179-210.

Jia, X., Williams, R.A., 2001. A packing algorithm for particles of arbitrary shapes. Powder Technology 120, 175-186.

Jia, X., Gan, M., Williams, R.A., Rhodes, D., 2007. Validation of a digital packing algorithm in predicting powder packing densities. Powder Technology 174, 10-13.

Johnson, S., Williams, J.R., Cook, B., 2004. Contact resolution algorithm for an ellipsoid approximation for discrete element modeling. Engineering Computations 21, 215-234.

Kleinhans, M.G., Jeukens, C.R.L.P.N., Bakker, C.J.G., Frings, R.M., 2008. Magnetic Resonance Imaging of coarse sediment. Sedimentary Geology 208, 69-78.

Koltermann, C.E., Gorelick, S.M., 1995. Fractional packing model for hydraulic conductivity derived from sediment mixtures. Water Resources Research 31, 3283-3297.

Korte, A.C.J.de, Brouwers, H.J.H., 2013. Random packing of digitized particles. Powder Technology 233, 319-324.

Krumbein, W.C., 1941. Measurement and geological significance of shape and roundness of sedimentary particles. Journal of Sedimentary Research 11, 64-72.

Latham, J.P., Lu, Y., Munjiza, A., 2001. A random method for simulating loose packs of angular particles using tetrahedra. Géotechnique 51, 871-879.

Lu, G., Third, J.R., Müller, C.R., 2012. Critical assessment of two approaches for evaluating contacts between super-quadric shaped particles in DEM simulations. Chemical Engineering Science 78, 226-235.

Matsushima, T., Katagiri, J., Uesugi, K., Tsuchiyama, A., Nakano, T., 2009. 3D shape characterization and image-based DEM simulation of the lunar soil simulant FJS-1. Journal of Aerospace Engineering 22, 15-23.

Ouchiyama, N., Tanaka, T., 1984. Porosity estimation for random packings of spherical particles. Industrial and Engineering Chemistry Fundamentals 23, 490-493.

Richard, P., Philippe, P., Barbe, F., Bourlès, S., Thibault, X., Bideau, D., 2003. Analysis by X-ray microtomography of a granular packing undergoing compaction. Physical Review E 68, 020301, doi: 10.1103/PhysRevE.68.020301.

Scott, G.D., 1960. Packing of spheres: packing of equal spheres. Nature 188, 908-909.

Song, Y.X., Turton, R., Kayihan, F., 2006. Contact detection algorithms for DEM simulations of tablet-shaped particles. Powder Technology 161, 32-40.

Suzuki, M., Oshima, T., 1985. Verification of a model for estimating the void fraction in a three-component randomly packed bed. Powder Technology 43, 147-153.

Tickell, F.G., Hiatt, W.N., 1938. Effect of angularity of grain on porosity and permeability of unconsolidated sands. The American Association of Petroleum Geologists 22, 1272-1274.

Vollmer, S., Kleinhans, M.G., 2007. Predicting incipient motion, including the effect of turbulent pressure fluctuations in the bed. Water Resources Research 43, W05410, doi: 10.1029/2006WR004919.

Wang, L.B., Park, J.Y., Fu, Y.R., 2007. Representation of real particles for DEM simulation using X-ray tomography. Construction and Building Materials 21, 338-346.

Weltje, G.J., Alberts, L.J.H., 2011. Packing states of ideal reservoir sands: Insights from simulation of porosity reduction by grain rearrangement. Sedimentary Geology 242, 52-64.

Wilcock, P.R., 1998. Two-fraction model of initial sediment motion in gravel-bed rivers. Science 280, 410-412.

Williams, J.R., Pentland, A.P., 1992. Superquadrics and modal dynamics for discrete elements in interactive design. Engineering Computations 9, 115-127.

Williams, S.R., Philipse, A.P., 2003. Random packings of spheres and spherocylinders simulated by mechanical contraction. Physical Review E 67, 051301, doi: 10.1103/PhysRevE.67.051301.

Wooster, J.K., Dusterhoff, S.R., Cui, Y.T., Sklar, L.S., Dietrich, W.E., Malko, M., 2008. Sediment supply and relative size distribution effects on fine sediment infiltration into immobile gravels. Water Resources Research 44, W03424, doi: 10.1029/2006WR005815.

Wu, W., Wang, S.S.Y., 2006. Formulas for sediment porosity and settling velocity. Journal of Hydraulic Engineering 132, 858-862.

Yu, A.B., Standish, N., 1991. Estimation of the porosity of particle mixtures by a linear-mixture packing model. Industrial and Engineering Chemistry Research 30, 1372-1385.

Zhang, W.L., Thompson, K.E., Reed, A.H., Beenken L., 2006. Relationship between packing structure and porosity in fixed beds of equilateral cylindrical particles. Chemical Engineering Science 61, 8060-8074.

Zhao, J., Li, S.X., Zou, R.P., Yu, A.B., 2012. Dense random packings of spherocylinders. Soft Matter 8, 1003-1009.

Zhou, Z.Y., Zou, R.P., Pinson, D., Yu, A.B., 2011. Dynamic simulation of the packing of ellipsoidal particles. Industrial and Engineering Chemistry Research 50, 9787-9798.

Zingg, T., 1935. Beitrag zur Schotteranalyse. Schweizerische Mineralogische und Petrographische Mitteilungen 15, 39-140.

Zou, R.P., Yu, A.B., 1996. Evaluation of the packing characteristics of mono-sized non-spherical particles. Powder Technology 88, 71-79.

## Figure captions

**Fig. 1.** Four unimodal (A, B, C, D) and three bimodal (E, F, G) grain size distributions used for the porosity measurements and simulations.

**Fig. 2.** Nine representative digitized particles in the 22.4-31.5 mm fraction of (A) Rhine sediments, and (B) Kall sediments, represented at a resolution of 0.5 mm/voxel.

**Fig. 3.** Shape properties of (A) Rhine sediments, and (B) Kall sediments in the Zingg classification. ($n = 9 \times 7 = 63$)

**Fig. 4.** Measured porosity for the Rhine sediments, Kall sediments and glass beads over the four unimodal distributions represented by logarithmic standard deviation (A) and three bimodal distributions represented by percentage of fine mode (B).

**Fig. 5.** Porosity difference between field measurements and laboratory measurements, based on the porosity data set provided by Frings et al. (2011). The study area was the 520 km long river reach between the barrage of Iffezheim (Rhine kilometer 334) and the German-Dutch border (Rhine kilometer 865).

**Fig. 6.** Generated digital packings for (A) Rhine sediments, (B) Kall sediments, and (C) glass beads. From left to right, the packings represent the four unimodal distributions (1, 3, 5, 7 fractions), and three bimodal distributions (30%, 50%, 70% proportion of fine mode).

**Fig. 7.** Comparison of model predictions with experimental data for each particle source over the four unimodal distributions (A, C, E) and three bimodal distributions (B, D, F).

**Fig. 8.** Comparison of model predictions with experimental data between the three different particle sources (i.e., the spherical glass beads, the sub-spherical Rhine sediments and the low-spherical Kall sediments) for a given grain size distribution. A to G represents the four unimodal distributions (1, 3, 5, 7 fractions), and three bimodal distributions (30%, 50%, 70% percentage of fine mode).

**Fig. 9.** Comparisons between relative errors over the four unimodal distributions (A), and three bimodal distributions (B).

**Fig. 10.** Cross section images of the generated digital packings for (A) Rhine sediments, (B) Kall sediments, and (C) glass beads. From left to right, the packings represent the four unimodal distributions (1, 3, 5, 7 fractions), and three bimodal distributions (30%, 50%, 70% percentage of fine mode).

**Fig. 11.** Sensitivity analysis of process control parameters on porosity, including (A) Rebounding probability, (B) Addition rate, and (C) Windup timesteps. Each simulation was conducted three times and the error bar shows 95% confidence interval for the simulated porosities.

**Table 1.** Set-up conditions applied in simulations

| Parameters | Values |
|---|---|
| Resolution | 0.5 mm/voxel |
| Container diameter | 104 mm |
| Dropping height | 300 mm |
| Sediment density | 2650 kg/m$^3$ |
| Glass density | 2500 kg/m$^3$ |
| Adding source | Rain-dropping mode |
| Rotation | Complete random |
| Rebounding probability | 0.35 |
| Addition rate | 1 particle/every 50 timesteps |
| Windup timestesps | 2000 |

**Table 2.** Porosity outcomes attained from laboratory measurements and simulations (a, standard deviation; b

| ID | Description of grain size distribution | | | Laboratory Measurements | | | |
|---|---|---|---|---|---|---|---|
| | | | | 1[#] | 2[#] | Mean | SD[a] |
| 1 | Rhine sediments | Unimodal distributions | 1 Fraction | 0.370 | 0.372 | 0.371 | 0.001 |
| 2 | | | 3 Fractions | 0.359 | 0.353 | 0.356 | 0.003 |
| 3 | | | 5 Fractions | 0.346 | 0.342 | 0.344 | 0.002 |
| 4 | | | 7 Fractions | 0.317 | 0.313 | 0.315 | 0.002 |
| 5 | | Bimodal distributions | 30%[b] | 0.272 | 0.267 | 0.270 | 0.003 |
| 6 | | | 50%[b] | 0.284 | 0.294 | 0.289 | 0.005 |
| 7 | | | 70%[b] | 0.300 | 0.297 | 0.299 | 0.002 |
| 8 | Kall sediments | Unimodal distributions | 1 Fraction | 0.383 | 0.380 | 0.382 | 0.002 |
| 9 | | | 3 Fractions | 0.385 | 0.380 | 0.383 | 0.003 |
| 10 | | | 5 Fractions | 0.368 | 0.364 | 0.366 | 0.002 |
| 11 | | | 7 Fractions | 0.331 | 0.324 | 0.328 | 0.004 |
| 12 | | Bimodal distributions | 30%[b] | 0.325 | 0.315 | 0.320 | 0.005 |
| 13 | | | 50%[b] | 0.316 | 0.317 | 0.317 | 0.001 |
| 14 | | | 70%[b] | 0.314 | 0.312 | 0.313 | 0.001 |
| 15 | Glass beads | Unimodal distributions | 1 Fraction | 0.365 | 0.362 | 0.364 | 0.002 |
| 16 | | | 3 Fractions | 0.383 | 0.377 | 0.380 | 0.003 |
| 17 | | | 5 Fractions | 0.368 | 0.368 | 0.368 | 0.000 |
| 18 | | | 7 Fractions | 0.353 | 0.344 | 0.349 | 0.005 |
| 19 | | Bimodal distributions | 30%[b] | 0.317 | 0.314 | 0.316 | 0.002 |
| 20 | | | 50%[b] | 0.314 | 0.310 | 0.312 | 0.002 |
| 21 | | | 70%[b] | 0.330 | 0.324 | 0.327 | 0.003 |

**Table 3.** Simulated porosity with varied rebounding probabilities (a, standard deviation)

| ID | Rebounding Probability | Addition Rate | | | Extra Timesteps | Windup Timesteps | Simulated porosity | | | | |
|---|---|---|---|---|---|---|---|---|---|---|---|
| | | Amount | Every Timesteps | Normal Timesteps | | | 1# | 2# | 3# | Mean | S |
| 1 | 0.1 | 1 | 10 | 7500 | 0 | 500 | 0.437 | 0.440 | 0.441 | 0.439 | 0 |
| 2 | 0.2 | 1 | 10 | 7500 | 0 | 500 | 0.433 | 0.436 | 0.436 | 0.435 | 0 |
| 3 | 0.3 | 1 | 10 | 7500 | 0 | 500 | 0.434 | 0.429 | 0.432 | 0.432 | 0 |
| 4 | 0.4 | 1 | 10 | 7500 | 0 | 500 | 0.434 | 0.429 | 0.430 | 0.431 | 0 |
| 5 | 0.5 | 1 | 10 | 7500 | 0 | 500 | 0.434 | 0.438 | 0.434 | 0.435 | 0 |
| 6 | 0.6 | 1 | 10 | 7500 | 0 | 500 | 0.433 | 0.433 | 0.438 | 0.435 | 0 |
| 7 | 0.7 | 1 | 10 | 7500 | 0 | 500 | 0.446 | 0.447 | 0.443 | 0.445 | 0 |

**Table 4.** Simulated porosity with varied addition rates (a, standard deviation)

| ID | Rebounding Probability | Addition Rate | | | Extra Timesteps | Windup Timesteps | Simulated porosity | | | | |
|---|---|---|---|---|---|---|---|---|---|---|---|
| | | Amount | Every Timesteps | Normal Timesteps | | | 1# | 2# | 3# | Mean | S |
| 1 | 0.25 | 1 | 2 | 1500 | 0 | 500 | 0.460 | 0.463 | 0.457 | 0.460 | 0 |
| 2 | 0.25 | 1 | 5 | 3750 | 0 | 500 | 0.446 | 0.448 | 0.441 | 0.445 | 0 |
| 3 | 0.25 | 1 | 10 | 7500 | 0 | 500 | 0.434 | 0.432 | 0.434 | 0.433 | 0 |
| 4 | 0.25 | 1 | 20 | 15000 | 0 | 500 | 0.424 | 0.427 | 0.428 | 0.427 | 0 |
| 5 | 0.25 | 1 | 30 | 22500 | 0 | 500 | 0.423 | 0.421 | 0.422 | 0.422 | 0 |
| 6 | 0.25 | 1 | 40 | 30000 | 0 | 500 | 0.421 | 0.421 | 0.420 | 0.421 | 0 |
| 7 | 0.25 | 1 | 50 | 37500 | 0 | 500 | 0.420 | 0.420 | 0.421 | 0.420 | 0 |

**Table 5.** Simulated porosity with varied windup timesteps (a, standard deviation)

| ID | Rebounding Probability | Addition Rate | | | Extra Timesteps | Windup Timesteps | Simulated porosity | | | | |
|---|---|---|---|---|---|---|---|---|---|---|---|
| | | Amount | Every Timesteps | Normal Timesteps | | | 1# | 2# | 3# | Mean | S |
| 1 | 0.25 | 1 | 10 | 7500 | 500 | 0 | 0.434 | 0.435 | 0.437 | 0.435 | 0 |
| 2 | 0.25 | 1 | 10 | 7500 | 500 | 1000 | 0.432 | 0.432 | 0.434 | 0.433 | 0 |
| 3 | 0.25 | 1 | 10 | 7500 | 500 | 2000 | 0.434 | 0.431 | 0.433 | 0.433 | 0 |
| 4 | 0.25 | 1 | 10 | 7500 | 500 | 4000 | 0.435 | 0.432 | 0.435 | 0.434 | 0 |
| 5 | 0.25 | 1 | 10 | 7500 | 500 | 8000 | 0.432 | 0.434 | 0.432 | 0.432 | 0 |
| 6 | 0.25 | 1 | 10 | 7500 | 500 | 16000 | 0.434 | 0.433 | 0.436 | 0.435 | 0 |
| 7 | 0.25 | 1 | 10 | 7500 | 500 | 32000 | 0.431 | 0.432 | 0.430 | 0.431 | 0 |

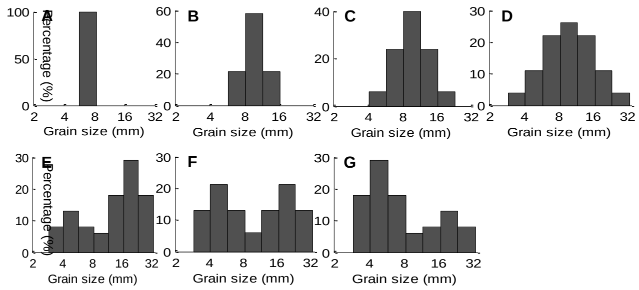


**Fig.1**

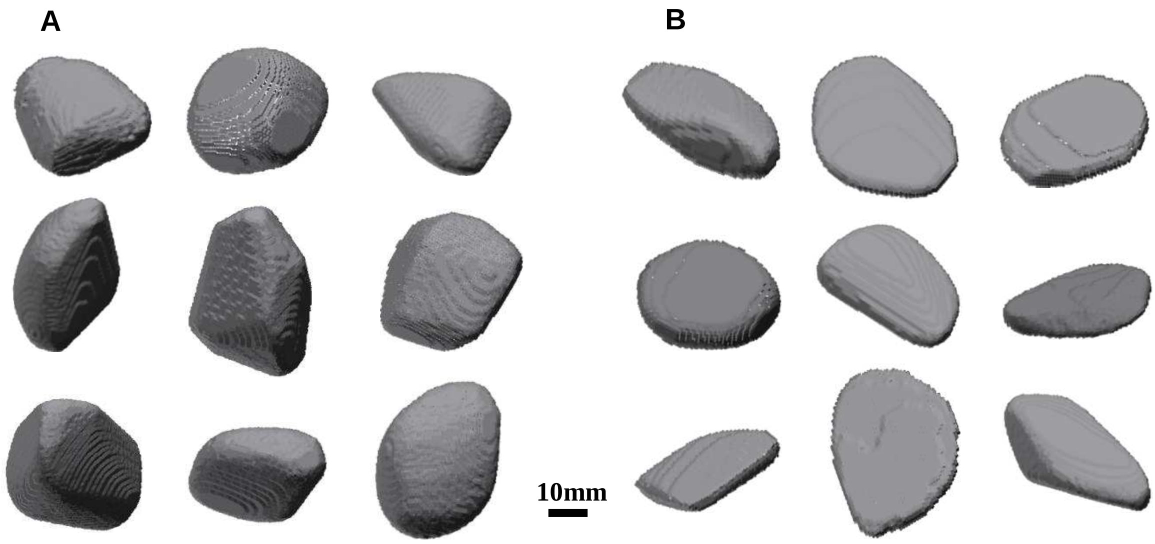


**Fig.2**

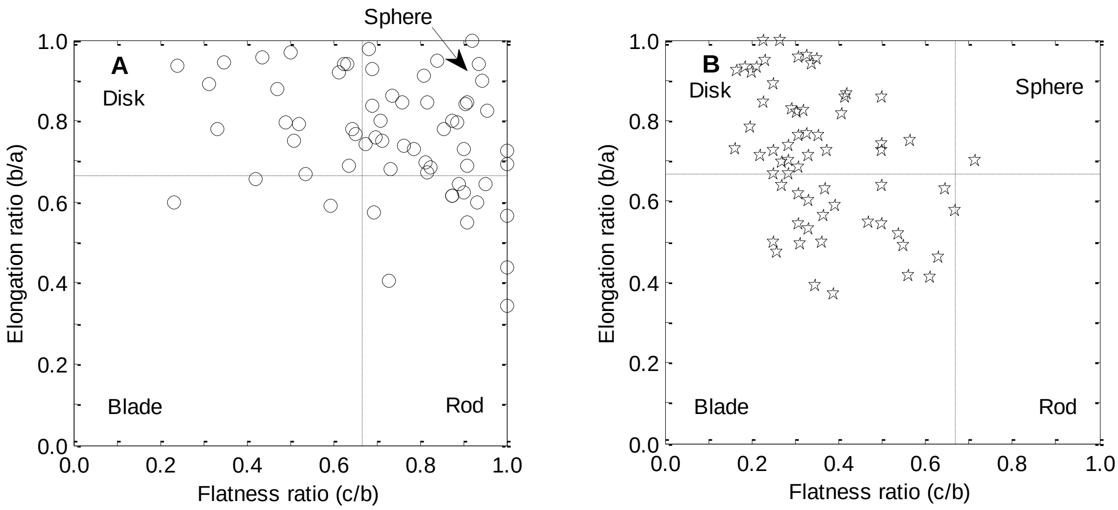
A
Sphere
Disk
Blade
Rod
Elongation ratio (b/a)
Flatness ratio (c/b)
B
Disk
Sphere
Blade
Rod
Elongation ratio (b/a)
Flatness ratio (c/b)

**Fig.3**

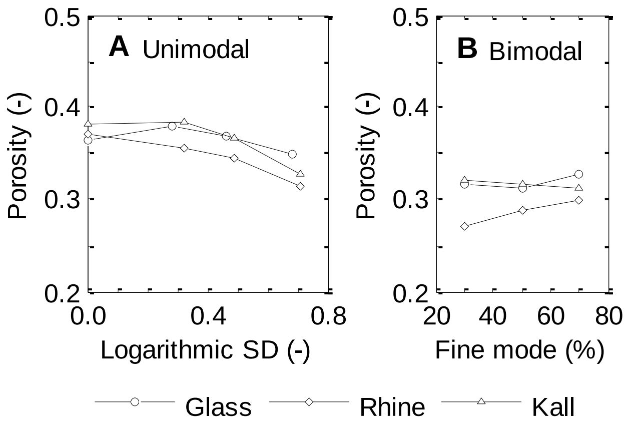
A Unimodal
B Bimodal
Porosity (-)
0.5
0.4
0.3
0.2
0.0
0.4
0.8
20
40
60
80
Logarithmic SD (-)
Fine mode (%)
Glass
Rhine
Kall

**Fig.4**

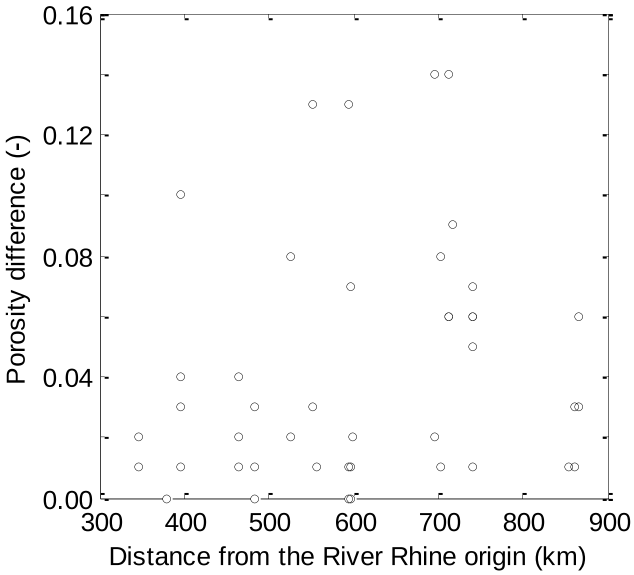
0.16
0.12
0.08
0.04
0.00
300
400
500
600
700
800
900
Porosity difference (-)
Distance from the River Rhine origin (km)

**Fig.5**

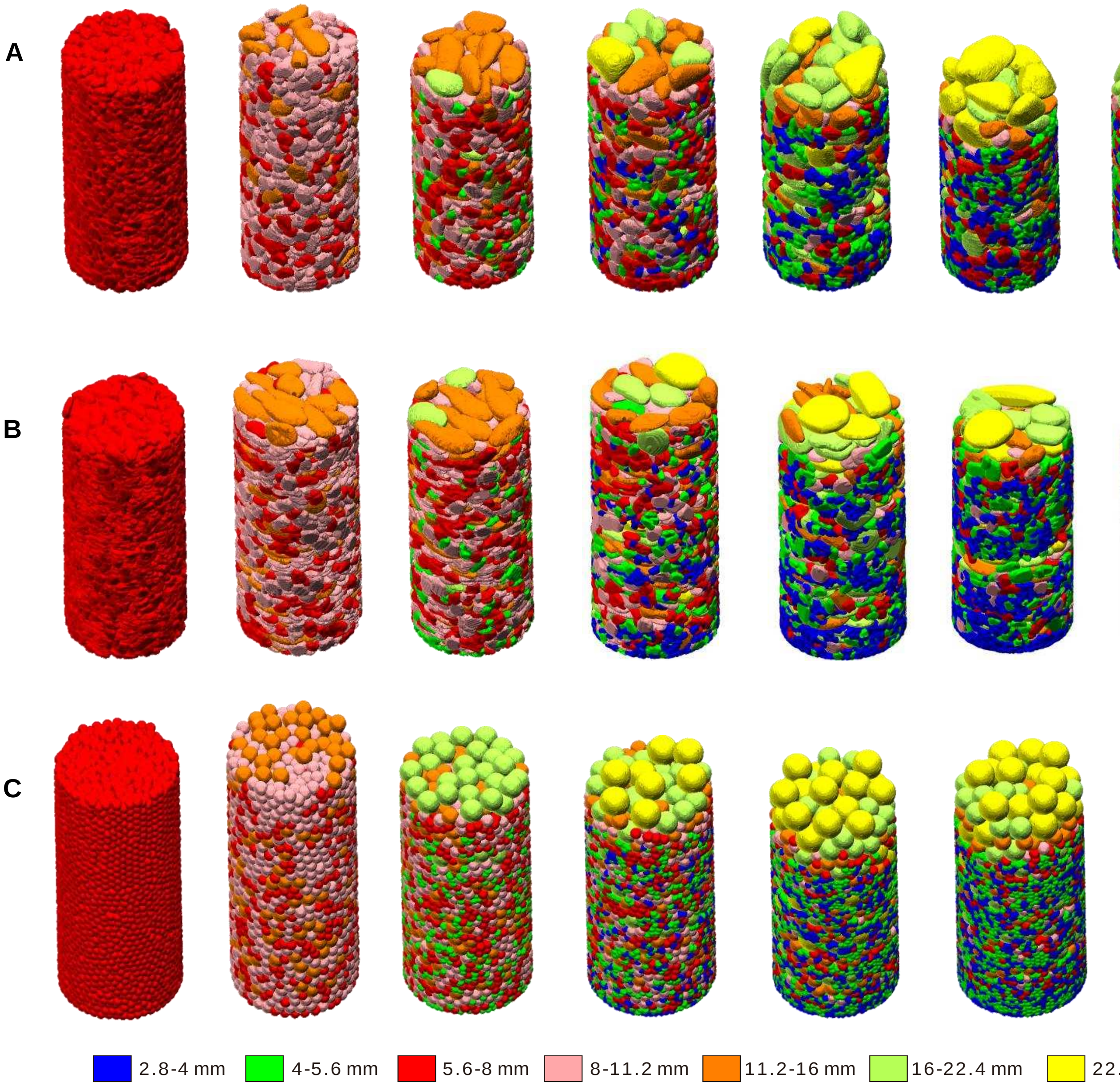


**Fig.6**

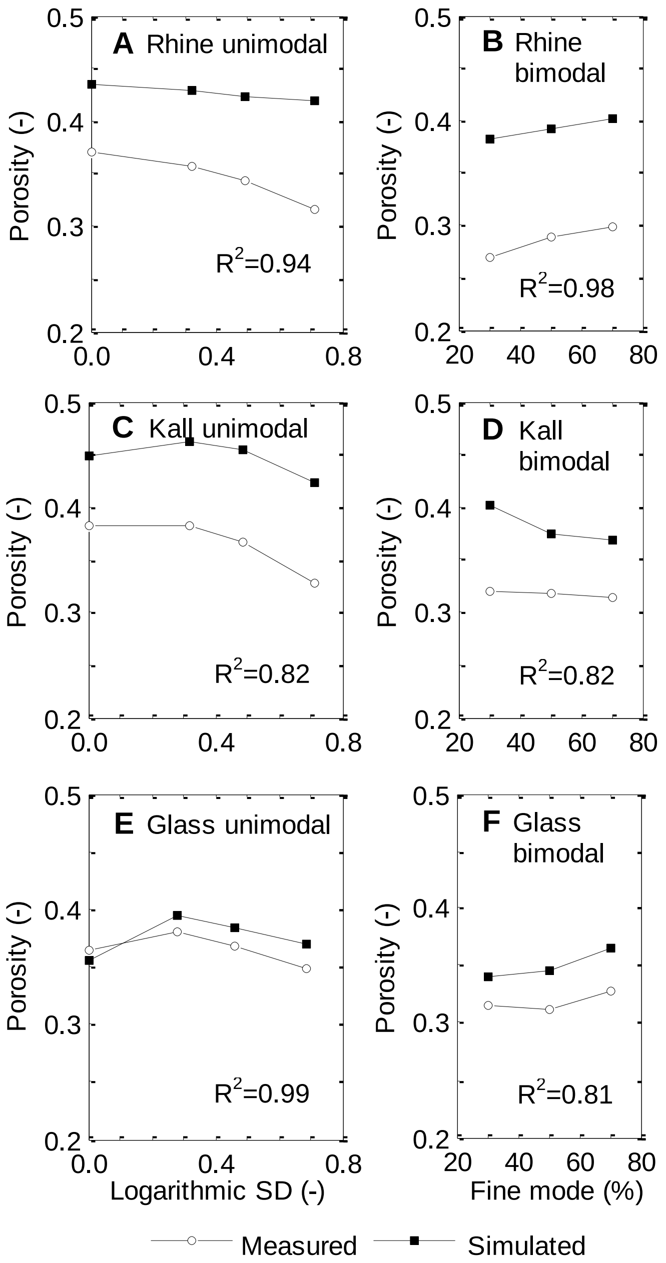
A Rhine unimodal
R2=0.94
B Rhine
bimodal
R2=0.98
C Kall unimodal
R2=0.82
D Kall
bimodal
R2=0.82
E Glass unimodal
R2=0.99
F Glass
bimodal
R2=0.81
Porosity (-)
Logarithmic SD (-)
Fine mode (%)
0.2
0.3
0.4
0.5
0.0
0.4
0.8
20
40
60
80
Measured
Simulated

**Fig.7**

619
620 **Fig.8**

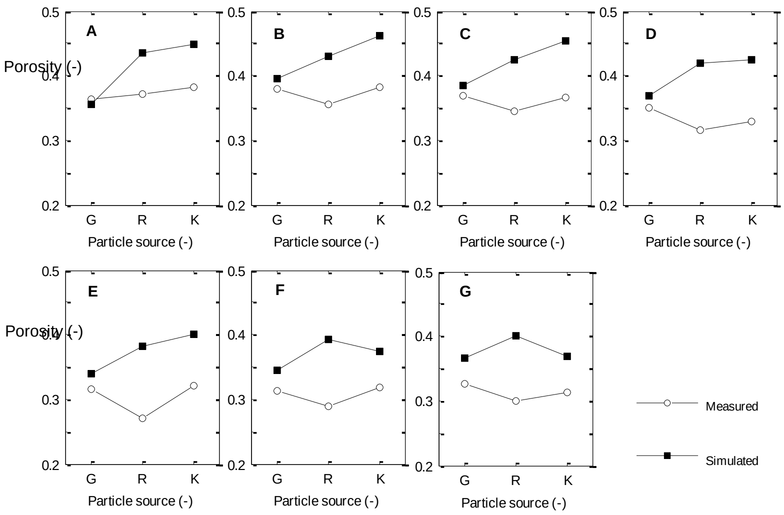


621

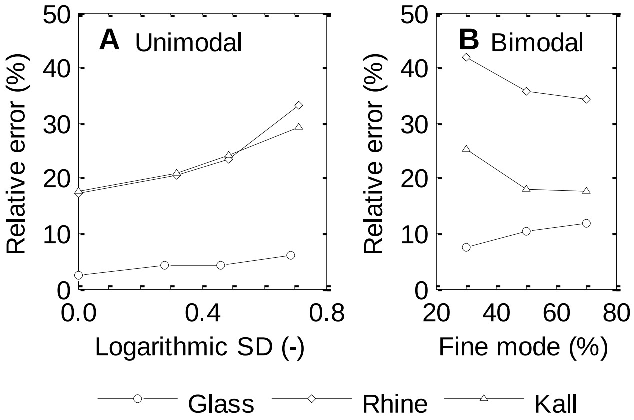


622
623 **Fig.9**

624

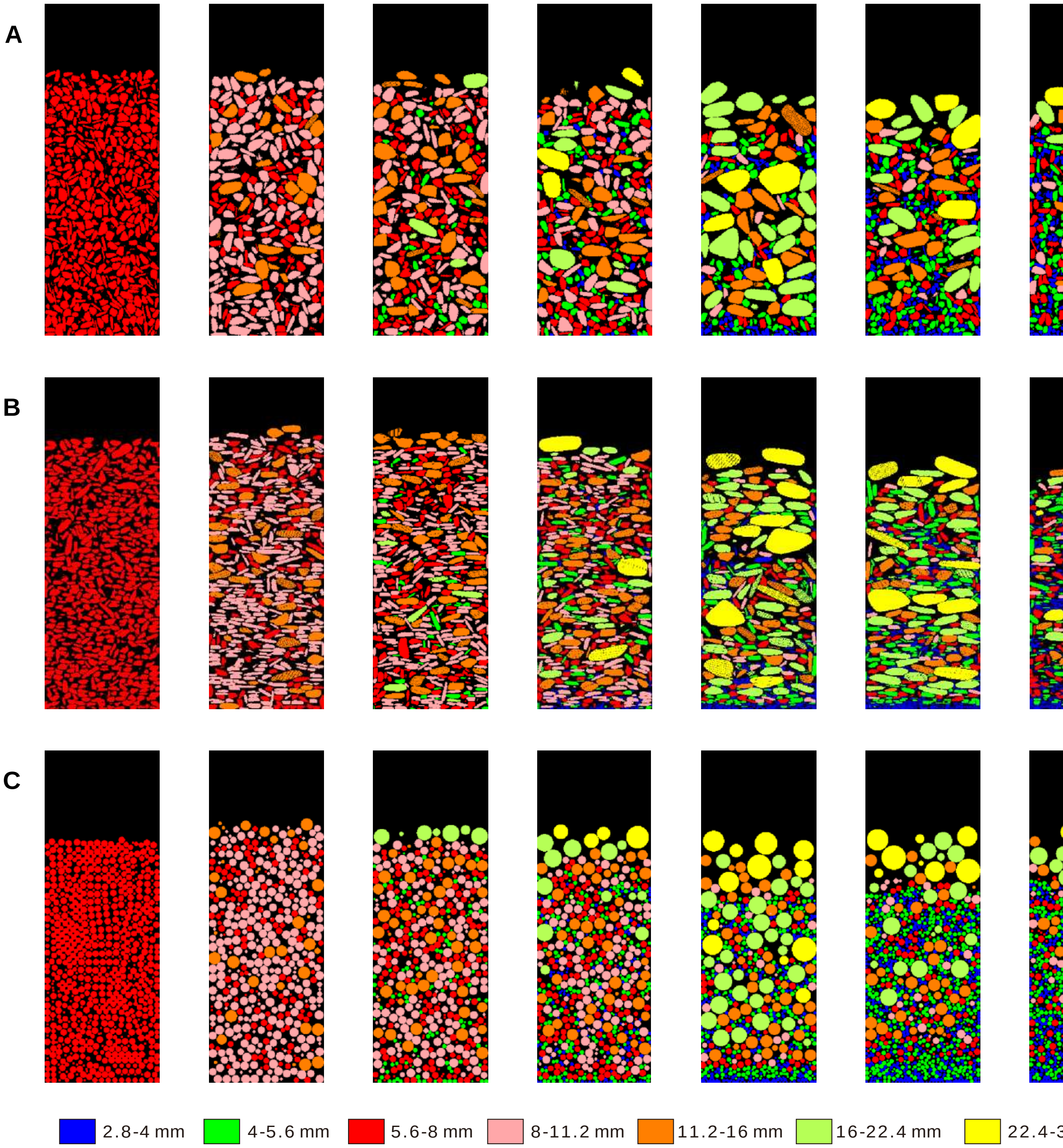


**Fig.10**

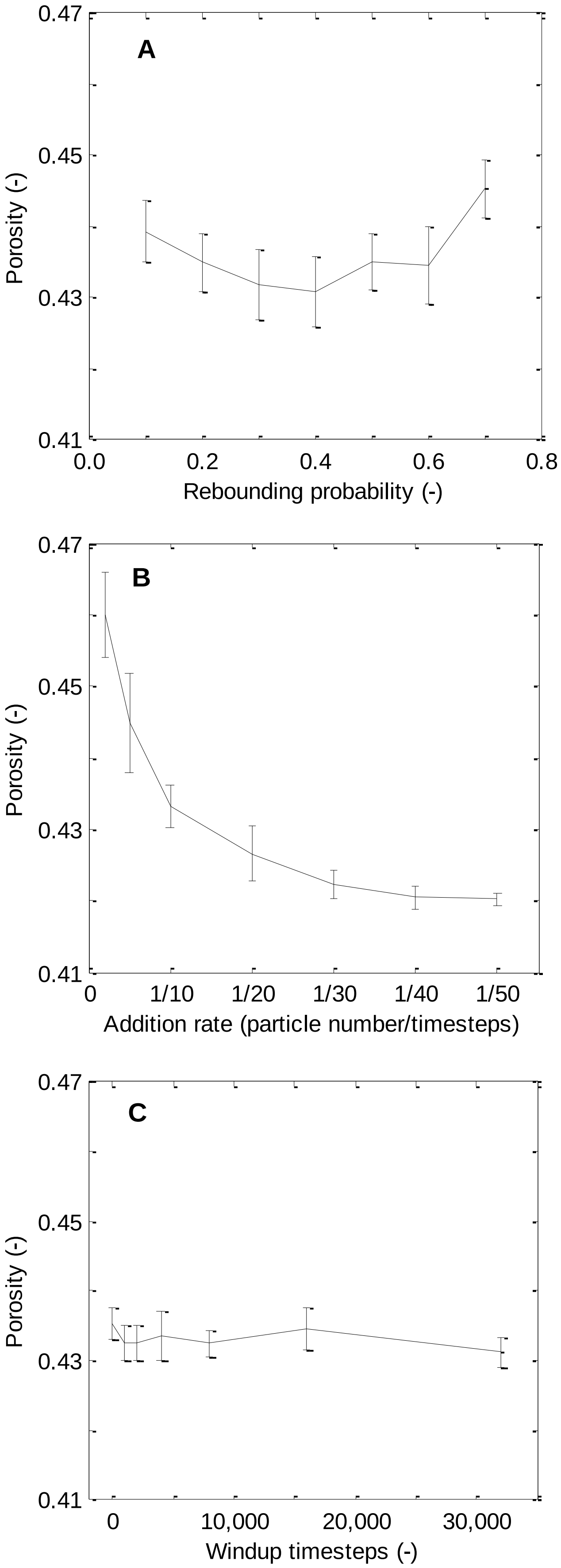
A
0.47
0.45
0.43
0.41
Porosity (-)
0.0
0.2
0.4
0.6
0.8
Rebounding probability (-)
B
0.47
0.45
0.43
0.41
Porosity (-)
0
1/10
1/20
1/30
1/40
1/50
Addition rate (particle number/timesteps)
C
0.47
0.45
0.43
0.41
Porosity (-)
0
10,000
20,000
30,000
Windup timesteps (-)

**Fig.11**